Society of Medical Education & Research

2026, Volume 6, Issue 1, Page No: 227-247

ISSN: 3108-4834

Archive of International Journal of Cancer and Allied Science

A Translatable circRNA Oncogene Drives Colorectal Cancer Liver Metastasis through a YAP-Dependent Feed-Forward Loop

Andrei Popescu[1]*, Mihai Ionescu[1], Elena Stan[2], Cristina Radu[3]

[1]Department of Colorectal Cancer Metastasis and circRNA, Faculty of Medicine, University of Bucharest, Bucharest, Romania.

[2]Department of YAP Signaling and Feed-Forward Loops, Faculty of Medicine, University of Agricultural Sciences Cluj-Napoca, Cluj-Napoca, Romania.

[3]Department of Liver Metastasis and Oncogene Translation, Faculty of Medicine, Polytechnic University of Bucharest, Bucharest, Romania.

***E-mail** ✉ andrei.popescu@usamv.ro

Abstract

Liver metastasis remains the predominant contributor to mortality in individuals diagnosed with colorectal cancer (CRC). Growing research highlights the significant involvement of circular RNA (circRNA) in driving cancer advancement. Nonetheless, the specific role of circRNA in the development of liver metastasis in CRC remains unclear. Circ-YAP expression levels were assessed by quantitative real-time PCR and in situ hybridization. Functional roles of circ-YAP were investigated using wound-healing assays, transwell migration/invasion assays, and CCK-8 proliferation assays. To explore the underlying molecular pathways through which circ-YAP facilitates CRC liver metastasis, RNA immunoprecipitation, RNA pull-down, luciferase reporter, and chromatin immunoprecipitation assays were performed. Additionally, an in vivo CRC liver metastasis model was developed to determine the influence of circ-YAP in animal systems. Circ-YAP was markedly elevated in CRC specimens with liver metastasis, and this elevation was strongly associated with unfavorable clinical outcomes. In vitro experiments demonstrated that circ-YAP enhanced the migratory and invasive capabilities of CRC cells. In vivo studies using patient-derived xenograft (PDX) models further confirmed its ability to promote liver metastasis. At the mechanistic level, circ-YAP produces a previously unidentified truncated protein, YAP-220aa, consisting of 220 amino acids. This protein competitively binds LATS1, thereby inhibiting YAP phosphorylation, promoting its nuclear localization, and subsequently stimulating the expression of multiple genes involved in metastasis. Notably, the N6-methyladenosine (m6A) modification plays a crucial role in enabling efficient translation of circ-YAP, relying on the m6A reader protein YTHDF3 and the eIF4G2-containing translation initiation complex. Furthermore, the YAP/TEAD complex was found to transcriptionally upregulate circ-YAP expression, thereby creating a positive feed-forward regulatory circuit. These results identify a novel oncoprotein, circ-YAP, that has not been previously described, suggesting its value as a potential biomarker and therapeutic target for managing liver metastasis in CRC patients.

Keywords: Circular RNA, Translation, N6-methyladenosine, Hippo signaling, Biomarker

Introduction

Colorectal cancer (CRC) is among the most frequent cancers affecting the gastrointestinal tract, occupying the third position in incidence and the second in mortality rates across all malignant neoplasms globally [1]. Metastatic spread is the chief reason for death in patients with CRC. In clinical practice, roughly 45–60% of CRC cases develop liver metastases, of which more than 90% are not amenable to surgical resection at initial diagnosis [2]. In patients with unresected liver metastases, the median survival is approximately 6.9 months, and the 5-year survival rate is below 5% [3]. Hence, unraveling the molecular mechanisms governing CRC liver metastasis and identifying innovative therapeutic targets is of

Access this article online https://smerpub.com/

Received: 28 March 2026; **Accepted:** 16 June 2026

How to cite this article: Popescu A, Ionescu M, Stan E, Radu C. A Translatable circRNA Oncogene Drives Colorectal Cancer Liver Metastasis through a YAP-Dependent Feed-Forward Loop. Arch Int J Cancer Allied Sci. 2026;6(1):227-47. https://doi.org/10.51847/ETWaoec2Cc

considerable clinical relevance for preventing metastatic progression and improving long-term patient survival.

Circular RNAs (circRNAs) represent a unique category of endogenous non-coding RNAs featuring a covalently closed circular conformation that lacks both the 5' cap and 3' poly(A) tail typical of linear mRNAs [4]. They are produced through back-splicing reactions catalyzed by the spliceosome, with individual genomic loci capable of generating single or multiple circRNA isoforms [5]. Analyses based on high-throughput sequencing and computational prediction have shown that circRNAs exhibit high evolutionary conservation and are expressed in highly specific patterns across disease states, tissue types, and cell lineages [6]. An expanding body of literature links circRNAs to the initiation and progression of multiple human disorders, with selected circRNAs emerging as reliable indicators of disease progression and patient prognosis [7, 8]. The modes of action employed by circRNAs are diverse and complex [9]. The best-characterized function involves their activity as miRNA sponges, with CDR1as serving as a classic example due to its capacity to bind over 70 miR-7 sites [10, 11]. Beyond this, various circRNAs interact directly with regulatory proteins, serving as molecular scaffolds or decoys to influence gene regulatory networks [12]. Of particular interest, accumulating findings reveal that certain circRNAs possess protein-coding potential and can generate functional peptides [13, 14]. One such example is the 173-amino-acid protein Nlgn-173aa, produced from circ-Nlgn, which functions as a transcription factor that contributes to myocardial fibrosis [15]. Similarly, truncated proteins derived from circRNAs, including E-Cad-254aa in glioma [16] and ARHGAP35-1289aa in hepatocellular carcinoma [17], have been implicated as key regulators in tumor biology. Because of their circular topology, circRNA translation proceeds cap-independent, often facilitated by internal ribosome entry sites (IRES) or m^6A modifications [18]. Among RNA modifications, N6-methyladenosine (m6A) is the most abundant in eukaryotic transcripts. This modification is reversible and governed by writer enzymes (METTL3/14 and WTAP), eraser proteins (FTO and ALKBH5), and reader proteins (YTHDF1/2/3 and YTHDC1/2) [19]. Although a small subset of circRNA-encoded microproteins has been functionally annotated, the biological significance of the majority remains to be investigated.

In the current investigation, we characterized circ-YAP as a critical promoter of liver metastasis in CRC. This circRNA encodes a 220-amino-acid open reading frame (ORF) and directs the synthesis of a novel YAP isoform, YAP-220aa, via m6A-mediated translation. Our data further indicate that YAP-220aa augments YAP pathway activity by interfering with LATS1-dependent phosphorylation of YAP, thereby preventing its cytoplasmic retention.

Materials and Methods

CRC tissues and cell lines

All colorectal cancer (CRC) specimens analyzed in this research were procured from Sun Yat-sen University Cancer Center. The collection comprised fresh-frozen samples (30 normal tissues, 23 primary CRC, 17 CRC cases with liver metastasis, 9 with lung metastasis, and 7 with brain metastasis) as well as formalin-fixed paraffin-embedded tissues (25 normal, 211 CRC, and 56 CRC with liver metastasis). Each participant provided written informed consent before sample collection. The Institutional Ethical Review Board of Sun Yat-sen University Cancer Center approved this study (SL-B2022-276-02). The human normal colonic epithelial cell line FHC (CRL-1831) and several CRC cell lines—HT-29 (HTB-38), SW480 (CCL-228), DLD1 (CCL-221), HCT116 (CCL-247), SW620 (CCL-227), and LoVo (CCL-229)—were purchased from the American Type Culture Collection (ATCC). These lines were routinely maintained in DMEM containing 10% fetal bovine serum (FBS). Additionally, TC71 patient-derived xenograft (PDX) cells were obtained from XENTECH (catalog No. XTM-233_CXT-399/R5700) and grown in advanced DMEM/F12 medium supplemented with 8% FBS, 1% antibiotics, and 1% glutamine. Periodic testing confirmed the absence of mycoplasma contamination in all cultures.

Quantitative real-time polymerase chain reaction (qRT-PCR)

Total RNA extraction was performed with TRIzol reagent (Invitrogen, CA, USA). One microgram of RNA served as the template for reverse transcription into cDNA using PrimeScript RT Enzyme (Takara Bio, Dalian, China). Subsequent amplification and quantification were performed using the TB Green Premix Ex Taq II Kit (Takara Bio).

Fluorescence in Situ Hybridization (FISH), In Situ Hybridization (ISH), and Immunohistochemistry (IHC)

A FAM-conjugated probe specific to the unique back-splice junction of circ-YAP was custom-designed and synthesized by GenePharma (Shanghai, China). FISH experiments followed the manufacturer's protocol provided with the FISH detection kit (GenePharma). For ISH analysis on paraffin-embedded sections, tissues underwent proteinase K digestion before overnight hybridization at 55 °C with a 5'-digoxigenin-labeled probe targeting the circ-YAP junction. Slides were then incubated overnight at 4 °C with anti-digoxigenin antibody (Roche, Basel, Switzerland), and signals were developed using NBT/BCIP substrate. IHC staining used a custom anti-YAP-220aa antibody (GenScript) at 1:50 and an anti-YAP antibody (#14,074, CST) at 1:400. Immunoreactivity was visualized with DAB. Scoring of ISH and IHC results was performed using the H-score system, as described previously [20].

Vectors, oligonucleotides, and transfection

Suppression of circ-YAP expression was accomplished through the CRISPR/Cas13d RNA-targeting system [21]. Three distinct sgRNAs directed against the circ-YAP back-splice junction were designed and synthesized (gRNA#1: TCCTTTCCTTAACAGGCCAGTACTGATGCA; gRNA#2: TCAGATCCTTTCCTTAACAGGCCAGTACTG; gRNA#3: TCCTTAACAGGCCAGTACTGATGCAGGCAC) before cloning into the pLKO.1 vector carrying RfxCas13d direct repeats. Lentiviruses were generated using psPAX2 and pMD2.G helper plasmids. Target CRC cells were transduced with 5 mg/mL polybrene and subsequently selected with 1.5 μg/mL puromycin. The circ-YAP overexpression construct was generated by synthesizing the full circ-YAP sequence and inserting it into the pLV-circ-Puro backbone, flanked by complementary sequences to facilitate circularization. For YTHDF3 gene knockout, three sgRNAs (gRNA#1: CTAAGCGAATATGCCGTAAT; gRNA#2: GTGGACTATAATGCGTATGC; gRNA#3: AAAGTTGACTCTTCTCGTAA) were cloned into a CRISPR/Cas9 All-in-One lentiviral vector, followed by transduction and isolation of single-cell clones. A short hairpin RNA (shRNA) targeting the YAP 3'-UTR (sequence: CCCAGTTAAATGTTCACCAAT) was constructed in the pLKO.1 lentiviral system, with stable lines established via lentiviral infection and puromycin selection. siRNAs targeting eIF4G2 and TEAD transcription factors were purchased from Ribobio (Guangzhou, China). Expression plasmids for YAP-5SA and YAP-5SA/S94A were sourced from Addgene. The m^6A consensus motif was mutated using the Q5 Site-Directed Mutagenesis Kit (New England Biolabs, CA, USA) following the supplier's instructions. All plasmid constructs underwent verification by Sanger sequencing. Transient transfections were performed with Lipofectamine 3000 (Invitrogen), and transfection efficiency was confirmed by qRT-PCR or Western blotting.

Wound healing, transwell, and CCK-8 assays

Cell migratory ability was evaluated using a standard wound-healing assay. CRC cells were seeded into 6-well culture plates, and uniform scratches were introduced with a sterile pipette tip. Cultures were then maintained in serum-free DMEM, and wound closure was documented after 24 hours. Invasion potential was assessed with Transwell chambers fitted with 8 μm pore-size membranes (BD Falcon, CA, USA). The lower compartment was filled with 600 μL of complete DMEM medium. After 24 hours of incubation, cells that had migrated through the membrane were fixed and stained with crystal violet. Cell viability and proliferation were measured by CCK-8 assay: cells were plated in 96-well plates and incubated with 10 μL of CCK-8 solution (Dojindo, Kumamoto, Japan) at 37 °C for 2 hours. Optical density was subsequently read at 450 nm on a microplate spectrophotometer.

Establishment of CRC liver metastasis model

A spontaneous liver metastasis model was developed by harvesting TC71 PDX cells (with or without circ-YAP depletion) using trypsin, followed by three washes in ice-cold PBS. Subsequently, 3×10^6 cells suspended in 50 μL PBS were orthotopically inoculated into the colonic subserosa of NOD/SCID mice. Ten weeks post-injection, the mice were sacrificed, and their livers were carefully removed for macroscopic and histological examination of metastatic deposits. In the experimental liver metastasis model, 1×10^6 TC71 PDX cells in 20 μL PBS were injected directly into the spleen. Four weeks after injection, metastatic nodules on the liver were enumerated. Liver metastatic burden was quantified as the total number of metastatic nodules multiplied by the average diameter of the lesions. All animal studies were performed with the approval of the Institutional Animal

Care and Use Committee of Sun Yat-sen University (SYSU-IACUC-2021-000653).

Western blot and co-immunoprecipitation (Co-IP)

Treated cells were rinsed thoroughly with cold PBS before lysis in RIPA buffer supplemented with a 1× protease inhibitor cocktail (Roche). Total protein concentration was measured using the Pierce™ BCA Protein Assay Kit (Invitrogen). Normalized protein samples were resolved on 8–10% SDS-PAGE gels and transferred to PVDF membranes. Following incubation with specific primary and HRP-conjugated secondary antibodies, protein bands were detected with Pierce™ ECL Western Blotting Substrate (Invitrogen). For Co-IP, cell lysates were pre-cleared with 20 μL of protein A/G agarose beads (Gibco, CA, USA). The cleared lysates were then incubated with the target primary antibody at 4 °C for 3 h, after which 40 μL protein A/G agarose beads were added for an additional 30 min at 4 °C. The immunoprecipitated complexes were separated by SDS-PAGE and analyzed by Western blot. Antibodies used included: anti-Flag (#80010-1-RR, Proteintech), anti-YAP-220aa (provided by GenScript), anti-METTL3 (#15073-1-AP, Proteintech), anti-YTHDF1 (#ab220162, Abcam), anti-YTHDF2 (#ab220163, Abcam), anti-YTHDF3 (#25537-1-AP, Proteintech), anti-eIF4G2 (#5169, CST), anti-eIF4A (#2013, CST), anti-eIF4B (#13,088, CST), anti-LATS1 (#3477, CST), anti-YAP (#14,074, CST), anti-14-3-3 (#9640, CST), p-YAP (S127) (#13,008, CST), anti-TEAD1 (#12,292, CST), anti-Tubulin (#11224-1-AP, Proteintech), anti-CDX2 (#ab76541, Abcam), anti-GAPDH (#60004-1-Ig, Proteintech), and anti-Histone H3 (#ab1791, Abcam).

Immunofluorescence (IF)

CRC cells were fixed in 4% paraformaldehyde, permeabilized with 0.1% Triton X-100, and blocked with 5% BSA for 30 minutes at ambient temperature. Primary antibodies against Flag, YAP-220aa, and YAP were applied overnight at 4 °C. After washing, cells were incubated with appropriate fluorescein-labeled secondary antibodies for 1 hour. Fluorescence images were captured with a fluorescence microscope, and nuclear counterstaining was performed with DAPI.

RNA immunoprecipitation (RIP) and methylated RNA immunoprecipitation (MeRIP)

The RIP procedure was carried out with the Magna RIP Kit (#17–700, Millipore, MA, USA) following the supplier's guidelines. Magnetic beads coated with anti-YTHDF3 antibody or control IgG (Millipore) were mixed with CRC cell lysates and incubated at 4 °C for 12 hours. After proteinase K treatment to release bound RNA, total RNA was isolated using TRIzol reagent, and circ-YAP enrichment was determined by qRT-PCR. MeRIP assays employed the Magna MeRIP™ m^6A Kit (17 − 10,499, Millipore). Total RNA was sheared into fragments of 100 nucleotides or shorter by heating at 70 °C for 5 minutes. These fragments were then incubated overnight at 4 °C with anti- m^6A antibody (#MABE1006, Millipore) and Magna Protein A/G Magnetic Beads. Bound RNA was eluted with m^6A 5′-monophosphate sodium salt, purified, and analyzed for circ-YAP levels via qRT-PCR.

RNA pull-down assay

In the in vivo RNA pull-down experiments, a biotin-conjugated oligonucleotide probe targeting the circ-YAP back-splice junction was prepared and incubated with CRC cells lysates at 4 °C for 5 hours. Streptavidin Magnetic Beads (Invitrogen) were subsequently introduced and incubated for 1 hour at 4 °C. Captured proteins were released and examined through Western blot analysis. For in vitro assays, linear circ-YAP transcripts were produced by in vitro transcription with the T7 Transcription Kit (Invitrogen) and biotinylated using Biotin RNA Labeling Mix (Roche), followed by circularization with T4 RNA ligase I. The biotin-labeled circ-YAP was then combined with recombinant human YTHDF3 protein (#ab166020, Abcam) in a binding buffer consisting of 20 mM Tris, 150 mM NaCl, 1% Triton X-100, 2 mM DTT, and 1 mM EDTA. Incubation occurred at 4 °C for 1 hour before addition of Streptavidin Magnetic Beads (Invitrogen), after which associated proteins were detected by Western blotting.

Detection of nascent circ-YAP

To monitor newly synthesized circ-YAP, cells were first treated with 5,6-dichlorobenzimidazole 1-β-D-ribofuranoside (DRB; Sigma-Aldrich, MO, USA) to inhibit ongoing transcription. Upon DRB withdrawal, 4-thiouridine (4sU; Sigma) was added to label newly generated RNA. Total RNA was harvested with TRIzol reagent, biotinylated, and isolated using Streptavidin Magnetic Beads (Invitrogen). Following thorough washing steps, the captured nascent transcripts were quantified for circ-YAP by qRT-PCR.

Luciferase reporter assay

YAP transcriptional activity was evaluated by transfecting cells stably depleted or overexpressing circ-YAP with the YAP-responsive reporter construct (8xGTIIC-luciferase, #34,615, Promega) via Lipofectamine 3000 (Invitrogen). Luciferase activity was quantified 48 hours later using the Dual-Luciferase Reporter Assay System (Promega) according to the manufacturer's instructions. Promoter activity of circ-YAP was examined by cloning either the complete or truncated promoter sequences into the pGL3-basic vector (Promega). These reporter plasmids were co-transfected along with pRL-TK and YAP-5SA constructs into recipient cells using Lipofectamine 3000 (Invitrogen). Relative luciferase values were measured following the same procedure. All conditions were tested in triplicate within 48-well culture plates.

Chromatin immunoprecipitation (ChIP) and re-ChIP

The ChIP procedure used the SimpleChIP® Plus Sonication Chromatin IP Kit (#56,383, CST) according to the provided protocol. ChIP-grade antibodies included anti-YAP (#14,074, CST), anti-Pol II (#N-20, Santa Cruz Biotechnology), and anti-p-Pol II (S5) (#ab5408, Abcam). In re-ChIP experiments, initial immunoprecipitation was performed with anti-YAP antibody (#14,074, CST). The eluted DNA-protein complexes were treated with 10 mM DTT at 37 °C for 30 minutes, centrifuged, and the resulting supernatant was further immunoprecipitated using anti-TEAD1 antibody (#610,922, BD Biosciences). Enriched DNA fragments were analyzed by qPCR.

DNA pull-down assay

Biotinylated DNA probes specific to the circ-YAP promoter sequence were synthesized and incubated overnight at 4 °C with agitation in the presence of sonicated nuclear protein extracts. Streptavidin Magnetic Beads (Invitrogen) were added for 1 hour at 4 °C. After three wash cycles, the bound proteins were eluted using 1× loading buffer and subjected to Western blot detection of YAP and TEAD1.

Statistical analysis

Results are expressed as the mean ± standard deviation (SD). Differences between two selected groups were assessed using the two-tailed Student's t-test, with consideration of variance. Predictive performance was evaluated through receiver operating characteristic (ROC) curve analysis. Overall survival curves for CRC patients were plotted by the Kaplan-Meier method and compared using the log-rank test. All statistical visualizations and computations were performed using GraphPad Prism 7 (La Jolla, CA, USA). Statistical significance was defined as a p-value below 0.05.

Results and Discussion

Association of circ-YAP with liver metastasis in colorectal cancer

To pinpoint the major circRNAs capable of translation in colorectal cancer (CRC) with liver metastasis, an integrated analysis of circRNA microarray profiling and ribosome nascent-chain complex-bound RNA sequencing was conducted. Common findings highlighted circ-YAP as a circRNA upregulated in CRC liver metastases and with translational potential. Gene set enrichment analysis (GSEA) further revealed a significant correlation between circ-YAP and liver-specific gene signatures. Evaluation of circ-YAP levels in fresh-frozen clinical specimens demonstrated modest upregulation in primary CRC tissues compared with normal counterparts. In contrast, substantially higher expression was evident in cases involving liver metastasis **(Figure 1a)**. Notably, circ-YAP expression showed no meaningful association with lung or brain metastases from CRC. Consistent with these observations, CRC cell lines possessing strong metastatic properties displayed elevated circ-YAP abundance **(Figure 1b)**. Characterization of its sequence revealed that circ-YAP is generated by back-splicing of exons 2 and 7 from the YAP pre-mRNA, resulting in a mature circular transcript measuring 842 bp **(Figure 1c)**. Unlike the corresponding linear transcript, circ-YAP proved resistant to RNase R digestion in both normal and malignant CRC cells **(Figure 1d)**. Additionally, circ-YAP exhibited remarkable stability, with a half-life exceeding 24 h **(Figure 1e)**. Subcellular localization studies using qRT-PCR and FISH confirmed that circ-YAP is primarily distributed in the cytoplasm **(Figure 1f)**.

Clinical relevance was further examined through in situ hybridization (ISH) on paraffin-embedded tissue sections. Circ-YAP expression was markedly increased in CRC samples with liver involvement **(Figures 1g and 1h)**, yielding an area under the curve (AUC) of 0.8433 (95% CI: 0.7645–0.9220) for distinguishing metastatic cases **(Figure 1i)**. Patients with elevated circ-YAP levels also had significantly poorer overall survival than those

with lower levels **(Figure 1j)**. The transcript remained stable across diverse pH conditions and multiple freeze-thaw cycles. Taken together, these results identify circ-YAP as an authentic circular RNA that holds promise as both a diagnostic biomarker and a prognostic indicator for CRC liver metastasis.

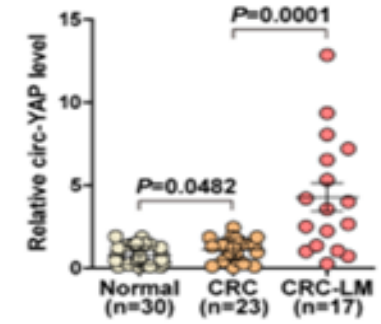

a)

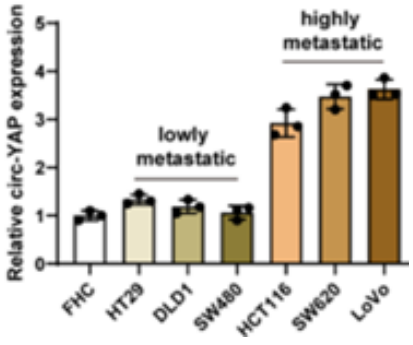

b)

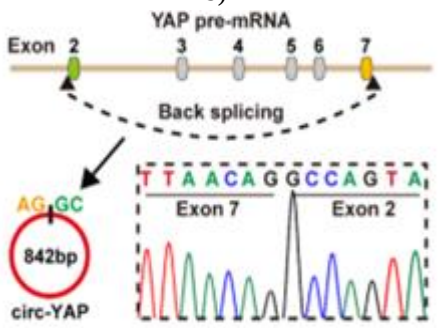

c)

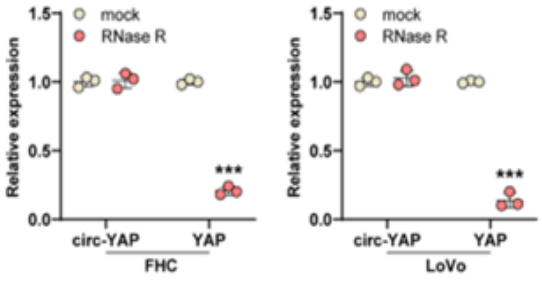

d)

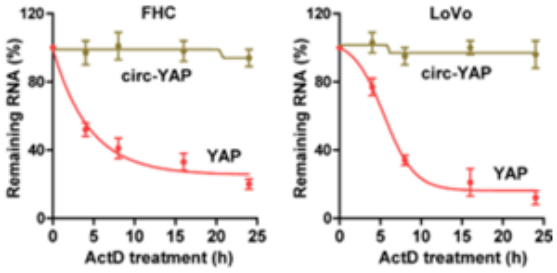

e)

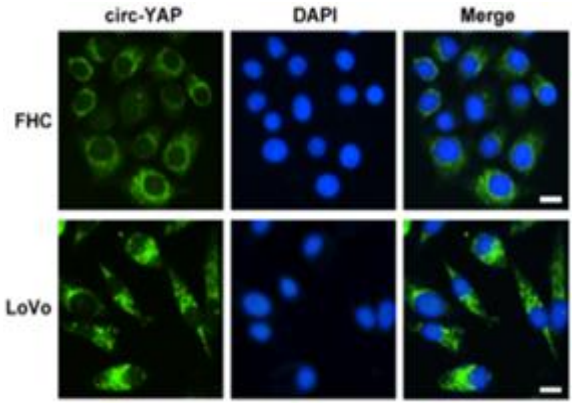

f)

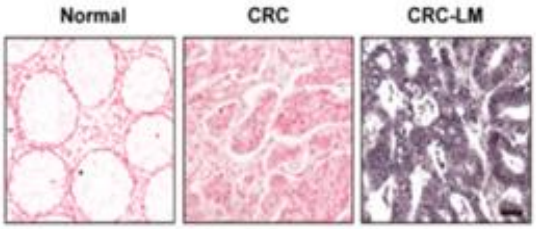

g)

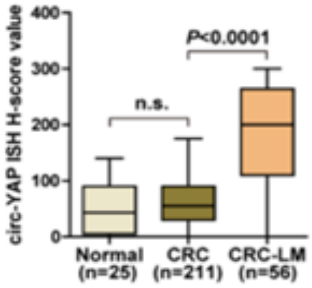

h)

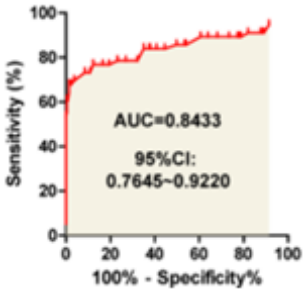

i)

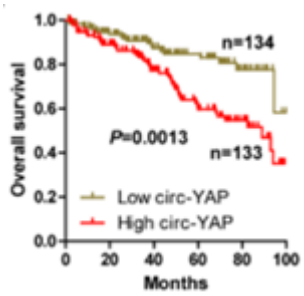

j)

Figure 1. Characterization of circ-YAP in colorectal cancer tissues with liver metastasis

(a, b) qRT-PCR quantification of circ-YAP expression across CRC tissues and cell lines, (c) Sanger sequencing validation of the back-splice junction in circ-YAP, (d, e) Following treatment of cells with 3U/μg RNase R or 5 μg/ml Actinomycin D, qRT-PCR was used to measure the abundance of circ-YAP and linear YAP mRNA, (f) FISH analysis of circ-YAP subcellular distribution, with DAPI nuclear staining. Scale bar, 25 μm. (g-i) ISH detection of circ-YAP in paraffin-embedded CRC tissues (g, h) and corresponding receiver operating characteristic (ROC) curve assessing predictive performance; (i) Positive circ-YAP signals appear dark purple. Scale bar, 50 μm, and (j) Kaplan–Meier survival analysis comparing CRC patients with low and high circ-YAP expression. *** $P < 0.001$. Values in (b, d, and e) are presented as the mean ± SD of three independent experiments, each performed in triplicate.

Depletion of circ-YAP attenuates liver metastatic burden in colorectal cancer

To define the functional contributions of circ-YAP, CRISPR/Cas13d was used to specifically suppress its expression. All three designed gRNAs efficiently reduced circ-YAP levels without influencing YAP mRNA abundance **(Figure 2a)**. Wound-healing and Transwell chamber experiments revealed that circ-YAP knockdown substantially impaired the migratory behavior of LoVo cells **(Figures 2b and 2c)** and their invasive properties **(Figures 2d and 2e)**. Parallel inhibitory outcomes were recorded in SW620 cells following circ-YAP depletion. In reciprocal experiments, forced expression of circ-YAP was introduced into CRC cell lines that naturally expressed low levels of this transcript **(Figure 2f)**. This upregulation markedly potentiated both migration and invasion **(Figures 2g and 2h)**. Of note, alterations in circ-YAP abundance had no impact on cellular proliferation, according to CCK-8 viability assays.

The biological relevance of these observations was further examined in vivo using a spontaneous liver metastasis patient-derived xenograft (PDX) model. This model was generated by direct implantation of TC71 PDX cells into the colonic submucosa of NOD/SCID mice **(Figure 2i)**. Ten weeks post-implantation, liver metastases were observed in 50% of control animals, in contrast to only 6.7% of mice in the circ-YAP knockdown cohort **(Figures 2j and 2k)**. An independent experimental metastasis assay involving intrasplenic injection of TC71 cells likewise confirmed that loss of circ-YAP significantly lessened hepatic metastatic load. Immunohistochemical detection of CDX2, an intestine-specific transcription factor, confirmed that the colonized cells in the liver originated from CRC rather than from resident hepatocytes or infiltrating immune populations. In summary, these results underscore the pivotal role of circ-YAP in driving CRC cell invasiveness and promoting liver metastasis.

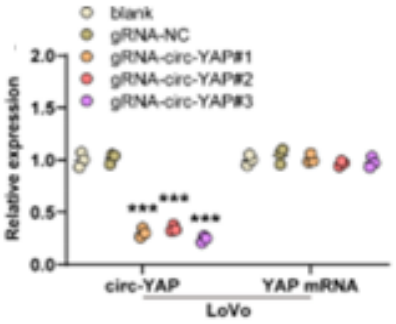

a)

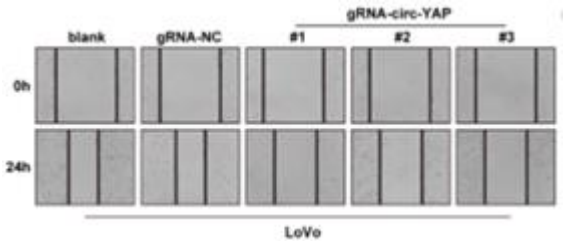

b)

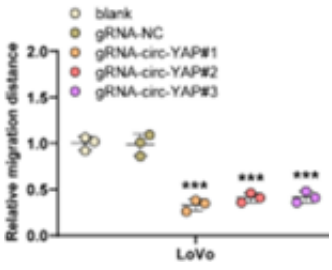

c)

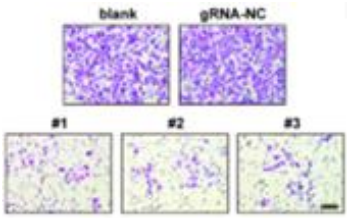

d)

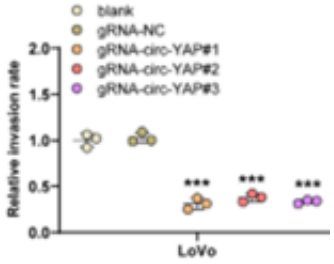

e)

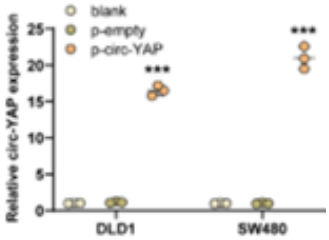

f)

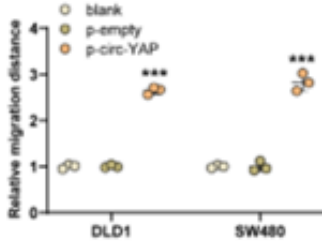

g)

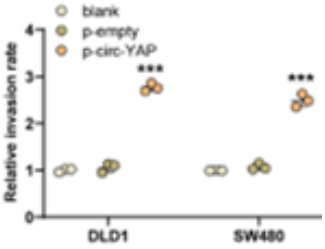

h)

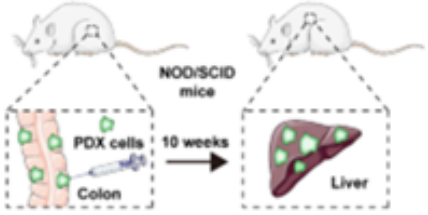

i)

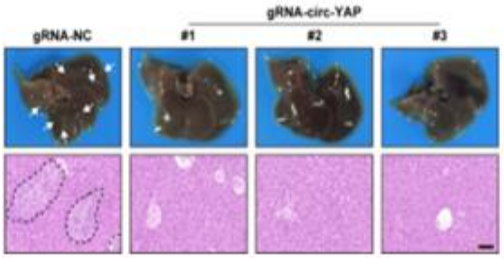

j)

CRC liver metastasis incidence

Parameter	gRNA-NC	gRNA-circ-YAP #1	gRNA-circ-YAP #2	gRNA-circ-YAP #3
Number	5/10	1/10	0/10	1/10
Percentage	50%	10%	0%	10%

k)

Figure 2. Inhibition of circ-YAP diminishes colorectal cancer liver metastasis burden

(a) qRT-PCR assessment of knockdown efficiency mediated by the specific sgRNAs, (b, c) Wound-healing assay examining migration following circ-YAP silencing in LoVo cells, (d, e) Transwell assay evaluating invasion capacity in circ-YAP-depleted CRC cells. Scale bar, 100 μm. (f) qRT-PCR confirmation of circ-YAP overexpression, (g, h) Migration and invasion analyses conducted in DLD1 and SW480 cells with elevated circ-YAP expression, (i) Schematic representation of the spontaneous liver metastasis model setup, (j) Typical images depicting liver metastatic foci in the respective experimental arms. Scale bar, 100 μm. (k) Percentage incidence of liver metastasis across the study groups. *** $P < 0.001$. Data (a, c, e, f, g, h) are expressed as the mean ± SD of three independent experiments performed in triplicate.

Circ-YAP produces a YAP-220aa protein isoform

Alignment of the circ-YAP sequence identified an open reading frame (ORF) spanning the back-splice junction and predicted to encode a 220-amino-acid protein **(Figures 3a and 3b)**. To experimentally confirm its coding ability, a Flag epitope tag was engineered into the circ-YAP overexpression plasmid in a manner that positioned the junction site near the ORF termination codon, splitting the Flag sequence across both sides of the circular RNA **(Figure 3c)**. Upon introduction into HEK293T cells, immunoblotting with an anti-Flag antibody revealed a specific band migrating at

approximately 26 kDa **(Figure 3d)**. This band displayed increased intensity following circ-YAP overexpression, as highlighted by Coomassie blue staining. The distinctive peptide sequence of the predicted protein was confirmed by mass spectrometry **(Figure 3e)**. A rabbit polyclonal antibody raised against this isoform successfully recognized the endogenous YAP-220aa protein **(Figure 3f)**.

Given that circRNA-encoded proteins are often produced through IRES elements or m^{6}A -driven mechanisms, the potential role of IRES sequences in circ-YAP was first examined. Two candidate IRES regions were tested using a dual-luciferase reporter system; however, neither construct altered the Luc/Rluc ratio compared with the empty vector control, excluding IRES-mediated translation. Instead, a conserved m^{6}A consensus motif ("GGACA") was located immediately upstream of the start codon **(Figure 3b)**. Substitution of the critical adenine to cytosine within this site **(Figure 3c)** virtually eliminated detectable Flag-tagged protein by western blot **(Figure 3d)**, demonstrating that m^{6}A modification is required for efficient translation of YAP-220aa. Subcellular fractionation and imaging showed that the YAP-220aa protein resides mainly in the cytoplasm **(Figure 3g)** and is preferentially expressed in CRC cell lines with elevated metastatic capacity **(Figure 3h)**. In agreement with these findings, depletion of the m^{6}A writer METTL3 substantially lowered endogenous YAP-220aa levels **(Figure 3i)**. At the same time, meRIP-qPCR showed higher m6A deposition on circ-YAP in highly metastatic cells than in those with lower metastatic potential **(Figure 3j)**.

In functional assays, forced expression of wild-type circ-YAP promoted migration and invasion of HT29 and SW480 cells, effects that were abrogated when the m^{6}A site was mutated **(Figures 3k and 3l)**. Correspondingly, in an experimental model of liver metastasis, wild-type circ-YAP enhanced metastatic outgrowth in the liver, whereas the m^{6}A -mutant variant did not **(Figure 3m)**. Taken together, these data indicate that circ-YAP contributes to CRC progression by generating a novel YAP protein isoform (YAP-220aa) via an m^{6}A -dependent translational process.

a)

b)

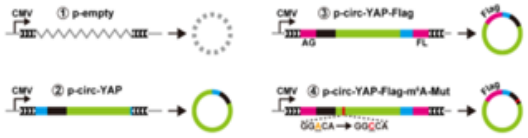

c)

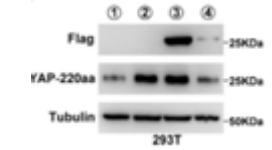

d)

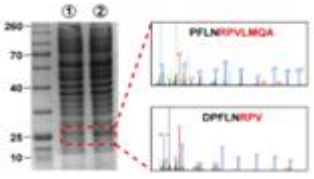

e)

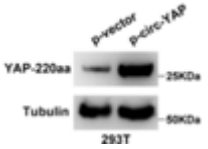

f)

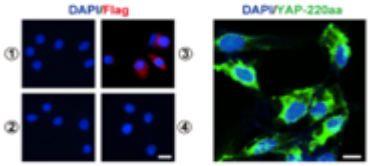

g)

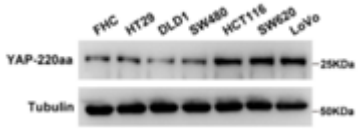

h)

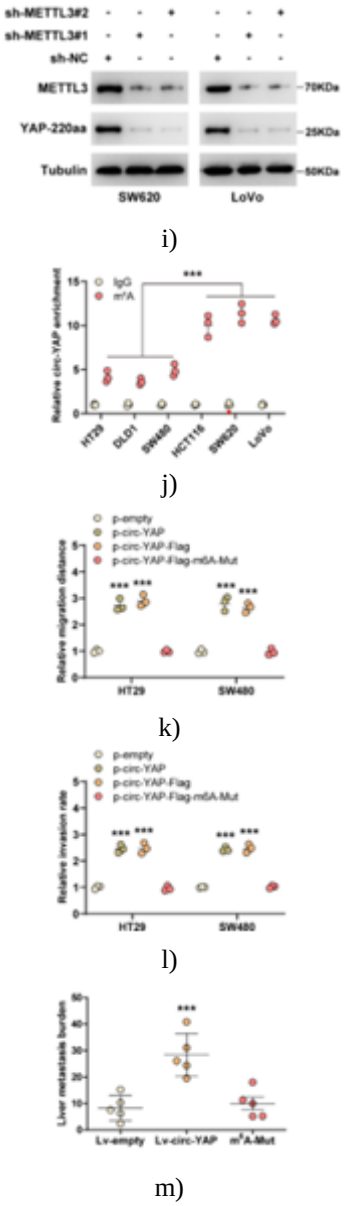

Figure 3. Circ-YAP encodes the YAP-220aa protein isoform in an m^{6}A -dependent manner

(a, b) Schematic representation and nucleotide sequence of circ-YAP, (c) Diagrams outlining the construction of the Flag-tagged and mutant vectors, (d) Western blot detection of Flag-tagged YAP-220aa protein in 293T cells after transfection with the respective plasmids, (e) Coomassie blue staining of protein lysates from control and circ-YAP-overexpressing cells, followed by mass spectrometric analysis of the excised band, (f) Western blot validation of endogenous YAP-220aa using the specific antibody, (g) Immunofluorescence detection of Flag and YAP-220aa localization in 293T cells. Scale bar, 25 μm, (h) Western blot analysis of YAP-220aa protein expression across a panel of CRC cell lines, (i) Western blot assessment of YAP-220aa levels upon METTL3 knockdown, (j) meRIP assay quantifying m^{6}A modification on circ-YAP in different CRC cell lines, (k, l) Evaluation of migratory and invasive abilities in HT29 and SW480 cells expressing the indicated constructs, and (M) In vivo liver metastasis assay comparing the metastatic potential of wild-type circ-YAP and its m^{6}A -mutant derivative (n = 5 per group).*** $P < 0.001$. Data (j, k, l) are shown as the mean ± SD of three independent experiments performed in triplicate. Uncropped western blot images are supplied in the Original Blot Image file.

The m^{6}A reader YTHDF3 is essential for translation of circ-YAP

We sought to identify which m^{6}A reader proteins mediate the translation of circ-YAP. As illustrated in **Figure 4a**, depletion of YTHDF3, but not of YTHDF1 or YTHDF2, substantially prevented the rise in YAP-220aa protein levels induced by circ-YAP overexpression **(Figure 4a)**. Notably, circ-YAP expression itself was unaltered by modulation of YTHDF1/2/3. To confirm the specific contribution of YTHDF3, we generated YTHDF3 knockout CRC cell lines via CRISPR/Cas9 gene editing. In these YTHDF3−/− LoVo and SW620 cells, the Flag-tagged translation product from p-circ-YAP-Flag was no longer detectable **(Figures 4b and 4c)**. In contrast, enforced expression of full-length YTHDF3 markedly enhanced YAP-220aa levels, whereas this stimulatory effect was lost when the active YTH domain was deleted **(Figure 4d)**.

Both RNA immunoprecipitation (RIP) and RNA pull-down experiments established a physical association between circ-YAP and YTHDF3 **(Figures 4e and 4f)**. Additionally, in vitro-transcribed circ-YAP incubated with recombinant GST-YTHDF3 protein demonstrated direct binding **(Figure 4g)**. Because eIF4G2 is known to participate in YTHDF3-dependent translational control [22], co-immunoprecipitation assays were conducted and confirmed the formation of an endogenous YTHDF3–eIF4G2 complex in SW620 and LoVo cells **(Figure 4h)**. Consistent with this, knockdown of eIF4G2 strongly reduced YAP-220aa protein abundance **(Figure 4i)**. RNA pull-down assays further showed that circ-YAP enriched eIF4G2 along with eIF4A/B. Still, these associations were completely abolished upon YTHDF3 deletion **(Figures 4j and 4k)**. Collectively, these data

indicate that circ-YAP recruits the eIF4G2-containing translation initiation machinery in a YTHDF3-dependent manner. Functionally, the promotive effect of circ-YAP on cell invasion was effectively abrogated by either YTHDF3 knockout or eIF4G2 silencing **(Figures 4l and 4m)**.

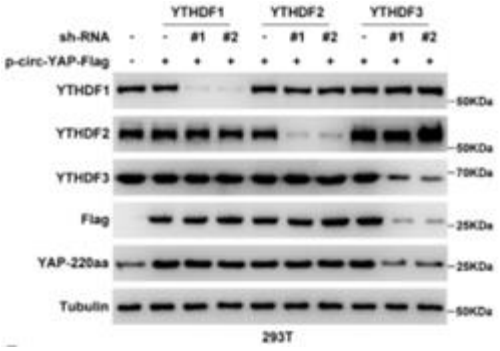

a)

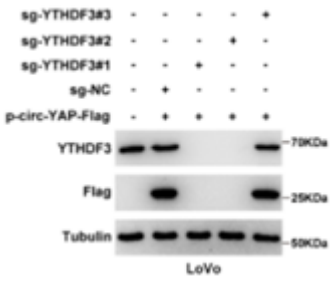

b)

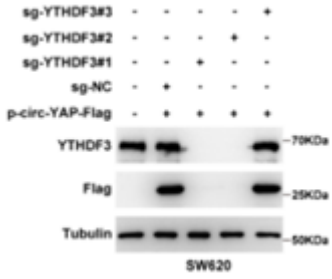

c)

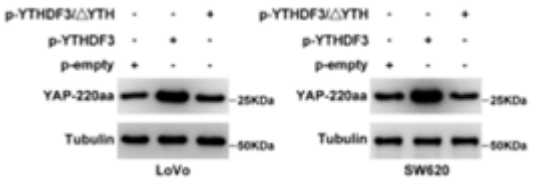

d)

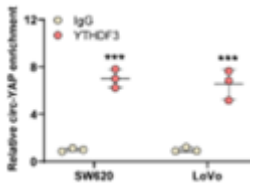

e)

f)

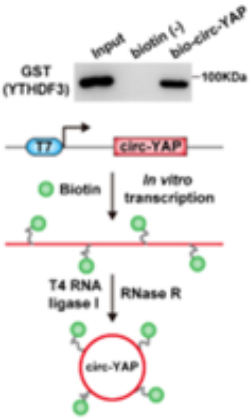

g)

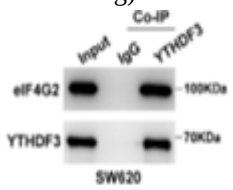

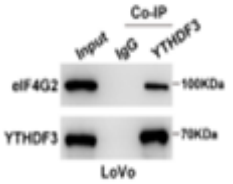

h)

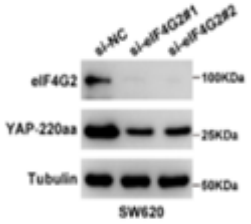

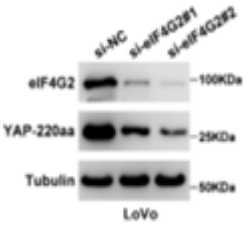

i)

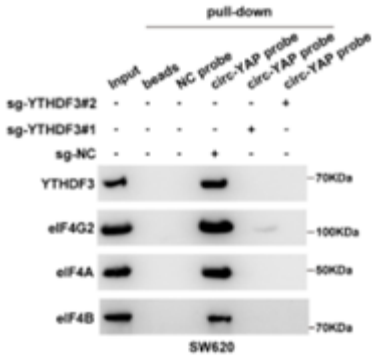

j)

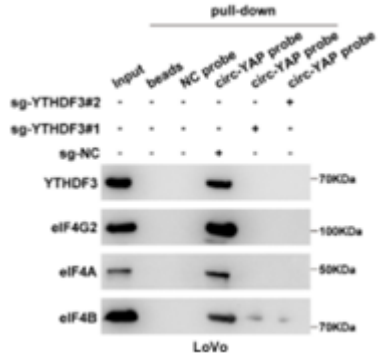

k)

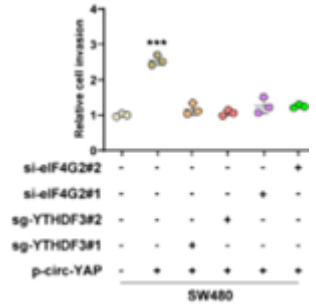

l)

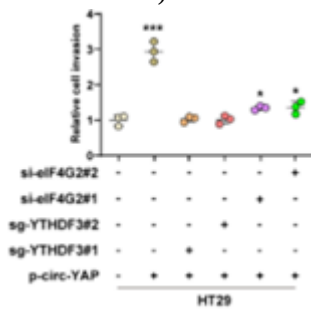

m)

Figure 4. YTHDF3 recruits the eIF4G2 complex to drive circ-YAP translation

(a) Western blot analysis of the indicated proteins in circ-YAP-overexpressing 293T cells following siRNA-mediated knockdown of YTHDF1/2/3, (b, c) Western blot showing the consequence of YTHDF3 knockout on YAP-220aa production, (d) LoVo and SW620 cells were transfected with the indicated constructs, and YAP-220aa levels were assessed by Western blot, (e) RIP assay performed with anti-YTHDF3 antibody and analyzed by qRT-PCR for circ-YAP enrichment, (f, g) In vivo and in vitro RNA pull-down assays using biotinylated circ-YAP probes, followed by Western blot detection of YTHDF3, (h) Co-IP assay demonstrating the interaction between endogenous YTHDF3 and eIF4G2, (i) Western blot analysis of YAP-220aa expression after eIF4G2 knockdown, (j, k) RNA pull-down assays with biotin-labeled circ-YAP in YTHDF3−/− SW620 and LoVo cells, followed by western blot for the indicated proteins, and (l, m) Transwell invasion assays in circ-YAP-overexpressing SW480 and HT29 cells upon YTHDF3 knockout or eIF4G2 depletion. * $P < 0.05$, *** $P < 0.001$. Data in panels e, l and m are presented as mean ± SD of three independent experiments performed in triplicate. Uncropped western blots are available in the Original Blot Image file.

YAP-220aa binds LATS1 and promotes nuclear localization of YAP

Examination of the YAP-220aa amino acid sequence showed that this peptide harbors the WW1/2 domain present in full-length YAP, a region known to mediate interaction with LATS1, leading to YAP phosphorylation and its subsequent cytoplasmic retention through 14-3-3 binding [23]. On this basis, we hypothesized that YAP-220aa may compete with YAP for LATS1, thereby attenuating YAP phosphorylation. In line with this prediction, anti-Flag immunoprecipitation in HEK293T cells expressing p-circ-YAP-Flag efficiently pulled down LATS1; however, this interaction was lost when the WW1/2 domain was removed **(Figure 5a)**. Endogenous complex formation between YAP-220aa and LATS1 was further validated in LoVo and SW620 cells **(Figures 5b and 5c)**. Depletion of circ-YAP significantly enhanced the association of YAP with LATS1 and 14-3-3 **(Figures 5d and 5e)**. In parallel, circ-YAP knockdown decreased YAP-220aa abundance and increased YAP phosphorylation in CRC cells; these alterations were rescued by restoration of wild-type circ-YAP but not by the m^6A site-mutated construct **(Figures 5f and 5g)**. Accordingly, forced expression of circ-YAP facilitated the translocation of YAP from the cytoplasm into the

nucleus, whereas introduction of the m^{6}A mutation prevented this shift **(Figures 5h and 5i)**.

YAP-dependent transcriptional activity measured by a luciferase reporter and the mRNA levels of its downstream pro-metastatic genes were substantially downregulated following circ-YAP silencing **(Figures 5j and 5k)**. Conversely, overexpression of wild-type circ-YAP—but not the m^{6}A -mutant form—produced the opposite outcome. At the functional level, the promotion of cell migration, invasion, and liver metastasis nodule formation by circ-YAP was markedly attenuated upon YAP silencing or pharmacological inhibition of YAP with verteporfin **(Figures 5l-5n)**. Collectively, these findings demonstrate that YAP-220aa encoded by circ-YAP drives CRC aggressiveness and hepatic metastasis by activating YAP signaling through competitive binding to LATS1.

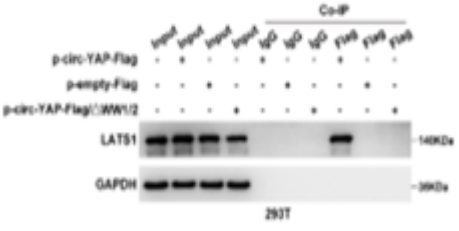

a)

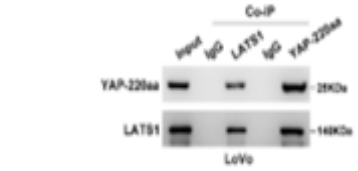

b)

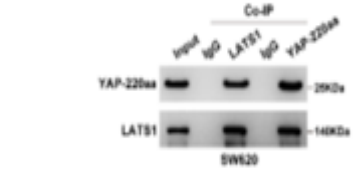

c)

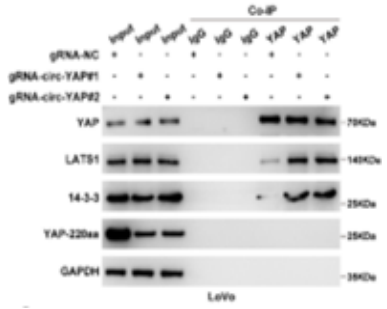

d)

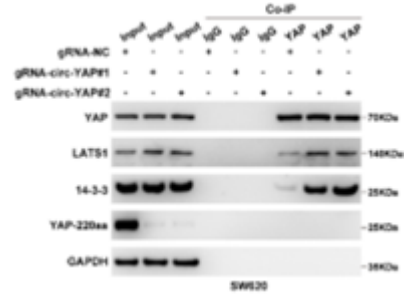

e)

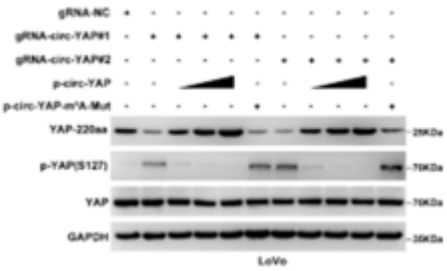

f)

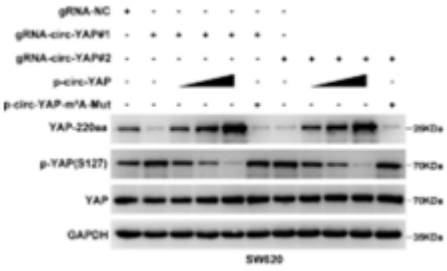

g)

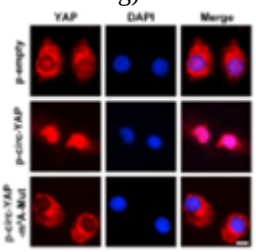

h)

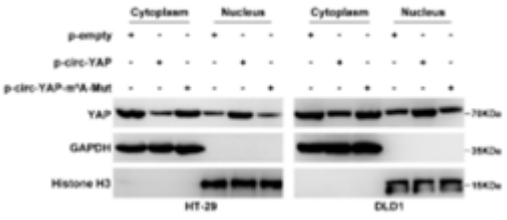

i)

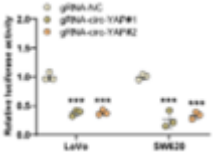

j)

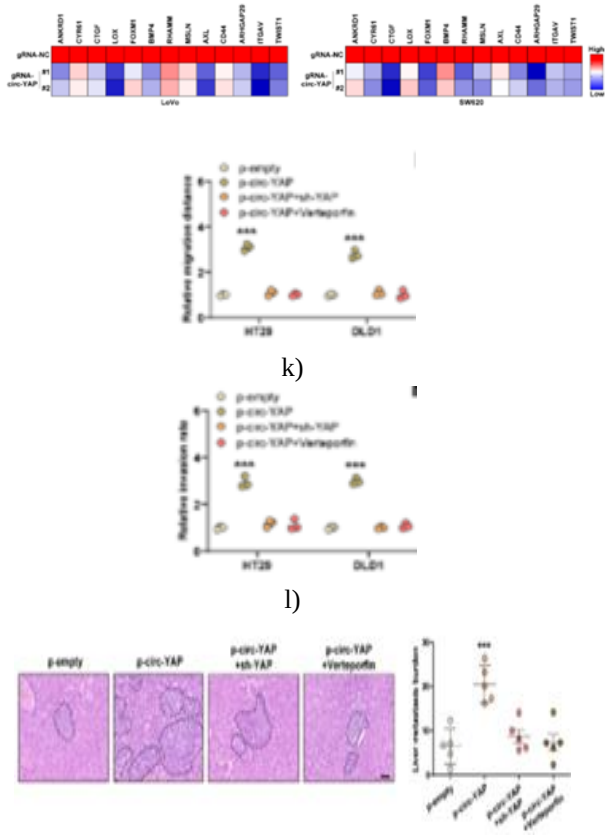

Figure 5. YAP-220aa augments YAP activity

(a-c) Co-IP experiments assessing the physical interaction between YAP-220aa and LATS1, (D, E) Co-IP experiments determining the binding of YAP to LATS1 and 14-3-3 in circ-YAP-depleted cells, (F, G) Western blot detection of the indicated proteins in circ-YAP-silenced LoVo and SW620 cells following rescue with wild-type or m^{6}A -mutated circ-YAP, (H, I) Immunofluorescence and subcellular fractionation Western blot analysis of YAP localization in circ-YAP-overexpressing cells. Scale bar, 25 μm. (J) Luciferase reporter assay measuring YAP transcriptional activity upon circ-YAP knockdown in CRC cells, (K) qRT-PCR quantification of YAP-regulated pro-metastasis genes after circ-YAP depletion, (L, M) Migration and invasion assays performed in HT29 and DLD1 cells after YAP knockdown or verteporfin exposure, and (N) Representative photographs and quantification of spontaneous liver metastatic burden (n = 5 per group). Scale bar, 100 μm. *** $P < 0.001$. Data (J, L, M) are shown as mean ± SD of three independent experiments conducted in triplicate. Uncropped western blot images are supplied in the Original Blot Image file.

YAP/TEAD complex transcriptionally activates circ-YAP

As a key transcriptional co-activator, YAP influences gene expression by partnering with TEAD family transcription factors (TEAD1–4) [24]. Remarkably, depletion of YAP or exposure to verteporfin resulted in a pronounced reduction of circ-YAP levels in both HEK293T cells and CRC cell lines **(Figure 6a)**. Ectopic expression of the constitutively active YAP-5SA mutant strongly upregulated circ-YAP. At the same time, variants lacking the transactivation domain (YAP-5SA/△C) or TEAD-binding capability (YAP-5SA-S94A) showed no such effect. Importantly, newly transcribed circ-YAP was similarly modulated by YAP manipulation and verteporfin **(Figure 6b)**, demonstrating transcriptional control of circ-YAP by YAP.

Mounting evidence suggests that select circRNAs are governed by autonomous promoter regions separate from their cognate linear transcripts. Inspection of ChIP-Seq datasets identified prominent TEAD binding within intron 1 of YAP pre-mRNA, implicating this segment as a potential promoter for circ-YAP. Subsequent cloning of promoter fragments into the pGL3-basic vector and luciferase assays localized YAP-responsive activity to the −974 to −374 upstream region relative to the circ-YAP transcription start site **(Figure 6c)**. Bioinformatic scanning with JASPAR uncovered two consensus TEAD motifs in this area (TB1: −886 ~ −877, sequence TAAATACTAT; TB2: −406 ~ −397, sequence CATATTCTTT) **(Figure 6d)**.

Individual mutations of TB1 or TB2 attenuated promoter-driven luciferase activity, and combined mutations of both sites completely negated the stimulatory effect of YAP-5SA **(Figures 6e and 6f)**. Rescue experiments further showed that YAP-5SA retained its ability to elevate circ-YAP in TEAD2-deficient cells but lost this capacity in cells lacking TEAD1, TEAD3, or TEAD4 **(Figures 6g and 6h)**, suggesting that TEAD1/3/4 are the primary mediators. ChIP-qPCR confirmed YAP occupancy at both TB1 and TB2 **(Figure 6i)**, along with concurrent enrichment of Pol II and its phosphorylated form **(Figures 6j and 6k)**, a critical step for transcriptional elongation.

ChIP-re-ChIP experiments established the presence of the YAP/TEAD1 complex at these sites on the circ-YAP promoter **(Figures 6l and 6m)**, which was independently validated through DNA pull-down using biotinylated probes **(Figure 6n)**. These findings collectively reveal

that YAP transcriptionally upregulates circ-YAP via TEAD, establishing a positive feedback circuit that facilitates CRC liver metastasis.

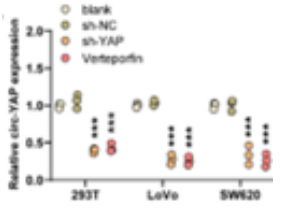

a)

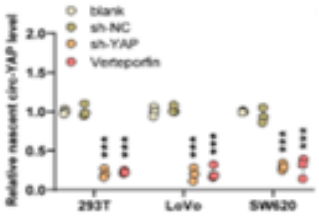

b)

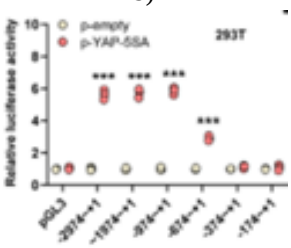

c)

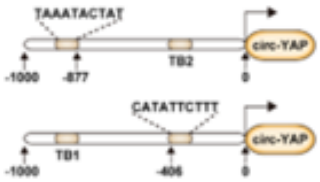

d)

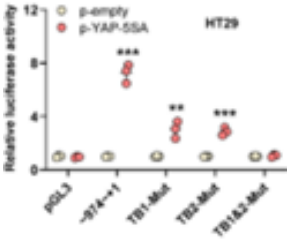

e)

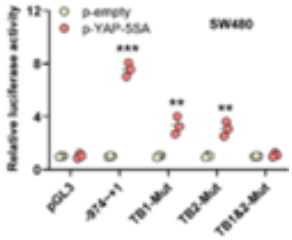

f)

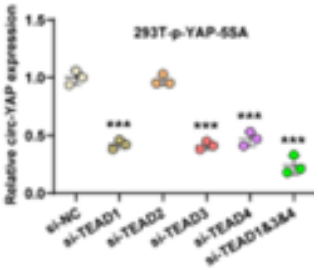

g)

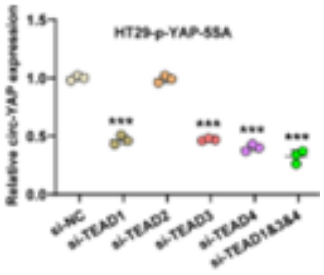

h)

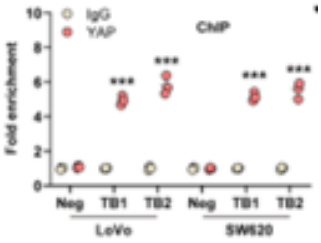

i)

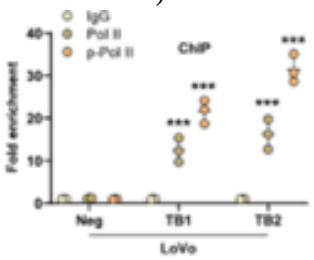

j)

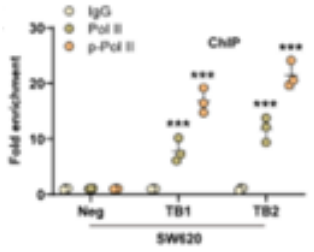

k)

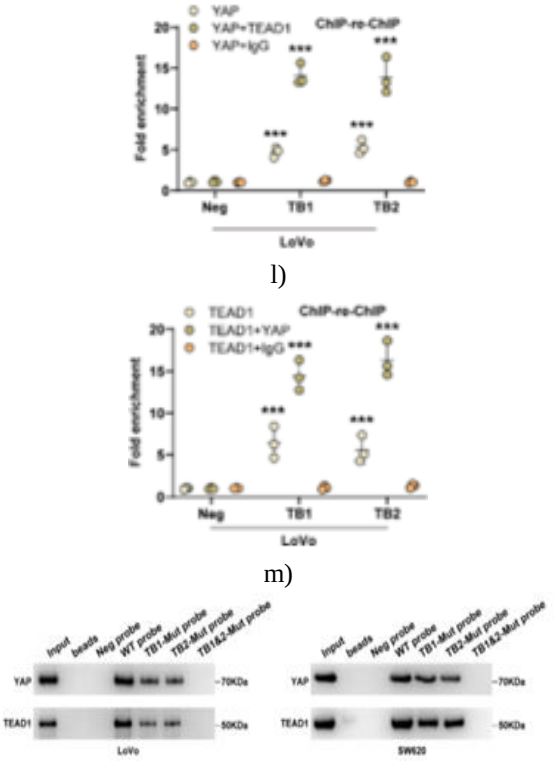

Figure 6. Transcriptional upregulation of circ-YAP by YAP

(a, b) qRT-PCR determination of total and nascent circ-YAP abundance in YAP-depleted or verteporfin-treated cells, (c) Luciferase reporter assays examining YAP-dependent activation of the circ-YAP promoter, (d) Location of two predicted TEAD binding elements in the circ-YAP promoter region, (e, f) Assessment of wild-type versus mutant circ-YAP promoter activity in HT29 and SW480 cells upon co-expression of p-YAP-5SA, (g, h) qRT-PCR analysis of circ-YAP expression in YAP-activated cells after silencing of specific TEAD members, (i-k) ChIP-qPCR detecting enrichment of YAP, Pol II, and p-Pol II at the circ-YAP promoter, (l, m) Sequential ChIP-re-ChIP-qPCR for co-recruitment of YAP and TEAD1 to the circ-YAP promoter, and (n) Biotinylated DNA pull-down followed by western blot analysis of YAP and TEAD1 binding to wild-type or mutated circ-YAP promoter probes in CRC cells. * $P < 0.05$, ** $P < 0.01$, *** $P < 0.001$. Data are presented as the mean ± SD from three independent experiments conducted in triplicate. Uncropped western blot images are supplied in the Original Blot Image file.

Clinical validation of the circ-YAP/YAP-220aa/YAP signaling axis

In the final set of analyses, expression of downstream YAP target genes was assessed in clinical CRC specimens. qRT-PCR data demonstrated significant positive correlations between circ-YAP abundance and multiple pro-metastatic transcripts, specifically CYR61, CTGF, TWIST1, and FOXM1 **(Figures 7a-7d)**. Immunohistochemical evaluation further revealed highly concordant expression patterns of circ-YAP and YAP-220aa in 92.5% of CRC cases, with discordance observed in only 7.5% **(Figures 7e and 7f)**. Elevated circ-YAP levels were also closely linked to prominent nuclear accumulation of YAP **(Figures 7e and 7g)**.

Consistent with these observations, western blotting of CRC tissues showed that specimens with high circ-YAP expression exhibited substantially increased YAP-220aa and nuclear YAP protein, together with decreased levels of phosphorylated YAP. YAP-220aa protein abundance was notably higher in primary CRC tumors associated with liver metastasis relative to those lacking metastatic spread **(Figure 7h)**. ROC curve analysis indicated strong discriminatory power, with an AUC value of 0.8597 (95% CI: 0.7616 ~ 0.9125) **(Figure 7i)**, supporting the potential utility of YAP-220aa as a predictive marker for CRC liver metastasis.

Survival analysis revealed that patients with concurrent high expression of circ-YAP and YAP-220aa had a markedly poorer prognosis than those with low levels of both molecules **(Figure 7j)**. These results suggest that integrating circ-YAP and YAP-220aa measurements offers enhanced prognostic stratification compared with circ-YAP assessment alone **(Figure 1j)**.

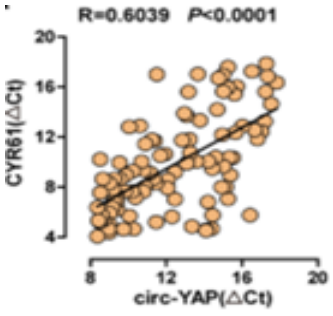

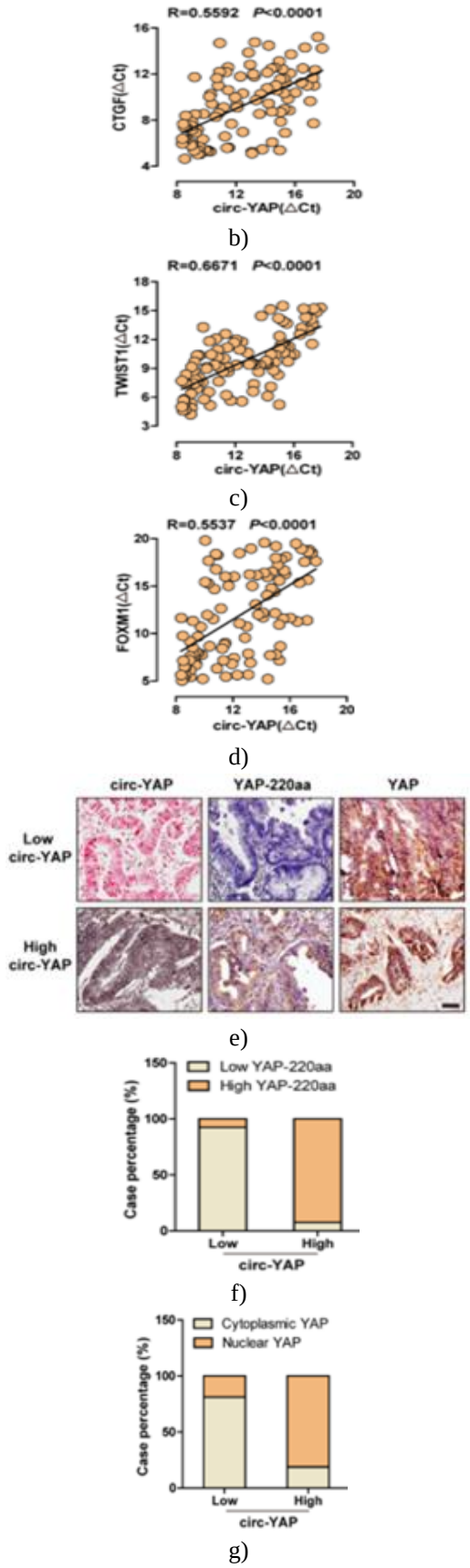

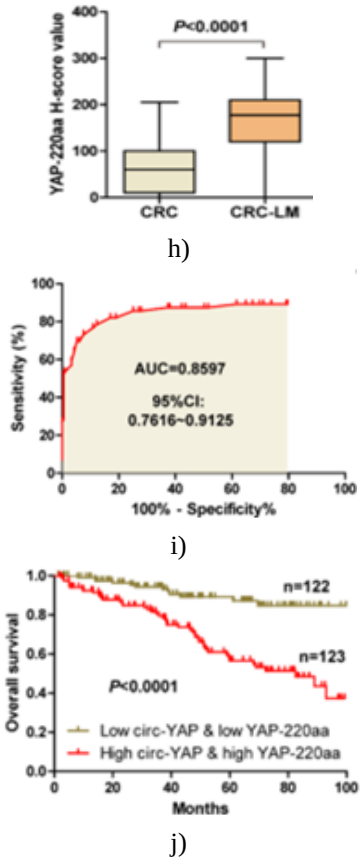

Figure 7. Clinical confirmation of the circ-YAP/YAP-220aa/YAP regulatory axis in patient samples

(a-d) Correlations of circ-YAP levels with the YAP downstream pro-metastatic genes CYR61, CTGF, TWIST1, and FOXM1 across 100 CRC specimens, (e-g) Representative ISH and IHC staining images for circ-YAP, YAP-220aa, and YAP in CRC tissues (e) along with quantitative statistical evaluation, (f, g) Scale bar, 100 μm, (h) IHC-based assessment of YAP-220aa expression in CRC cases with versus without liver metastasis, (i) ROC curve analysis demonstrating strong discriminatory power of YAP-220aa for predicting CRC liver metastasis, with an AUC value of 0.8597 (95% CI: 0.7616–0.9125), and (j) Kaplan-Meier survival analysis of CRC patients grouped according to combined high versus low circ-YAP and YAP-220aa expression.

CircRNAs have gained recognition as significant regulators of cancer biology. Although only a limited subset of circRNAs has been functionally annotated to date, the majority remain largely uncharacterized. Growing evidence indicates that certain circRNAs possess coding potential [25]; however, the contributions

of the resulting peptides or proteins to human malignancies, particularly CRC liver metastasis, remain poorly defined.

In this study, we identified for the first time a novel endogenous protein, YAP-220aa, translated from circ-YAP. This protein promotes CRC liver metastasis by interfering with LATS1-mediated phosphorylation of YAP, thereby enhancing YAP transcriptional activity. Mechanistic studies demonstrated that the m^{6}A reader protein YTHDF3 recognizes m^{6}A -modified circ-YAP and recruits the eIF4G2-containing translation initiation complex to facilitate its translation. Furthermore, the YAP/TEAD complex binds directly to the circ-YAP promoter region and drives its transcription, establishing a positive feedback loop between circ-YAP and YAP **(Figure 8)**.

Preclinical analyses showed that both circ-YAP and its translation product, YAP-220aa, effectively predict liver metastasis and overall survival in CRC patients, highlighting their potential clinical utility. Collectively, our results expand current understanding of the biological roles of circRNA-derived peptides and identify promising prognostic biomarkers and therapeutic targets for patients with CRC liver metastasis.

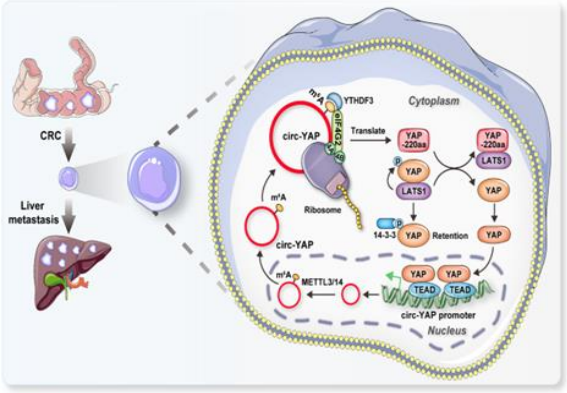

Figure 8. Schematic illustration depicting how circ-YAP promotes CRC liver metastasis.

circ-YAP is translated into the novel YAP isoform YAP-220aa in an m^{6}A -dependent manner. YAP-220aa then interacts with LATS1, disrupting the LATS1–YAP association. This leads to enhanced nuclear translocation of YAP, transcriptional activation of pro-metastatic genes and circ-YAP itself, and the establishment of a positive feedback regulatory loop.

CircRNAs exert diverse regulatory effects on biological processes in a highly context-dependent fashion [26]. Their subcellular distribution is a critical determinant of function: cytoplasmic circRNAs can sequester miRNAs, interact with various proteins, and undergo translation into functional peptides, whereas nuclear circRNAs may associate with DNA or transcription factors to influence gene expression [27]. Importantly, circRNA localization is dynamic rather than fixed, with profound implications for disease pathogenesis [28]. For example, under cellular stress, circ-C9ORF72 translocates from the nucleus to the cytoplasm, where its export contributes to neurological and neuromuscular disorders by producing dipeptide repeat proteins [29].

In the present work, circ-YAP was found to localize predominantly in the cytoplasm of both normal and CRC cells as well as in clinical tissues, indicating that altered spatiotemporal distribution is unlikely to drive CRC initiation. Instead, circ-YAP serves as a template for translation of the novel protein YAP-220aa, a process dependent on m^{6}A modification. It is well recognized that m^{6}A represents one of the most abundant RNA modifications in eukaryotic cells, with specific writers, erasers, and reader proteins identified [30]. Dysregulation of these enzymes has been implicated in various pathologies, including cancer, neurological disorders, and developmental defects [31, 32]. The m^{6}A modification typically occurs within the consensus sequence “RR m^{6}A CH” (R = G or A; H = A, C, or U) and modulates multiple aspects of RNA metabolism, including stability, splicing, polyadenylation, nuclear export, and translation [33].

We identified a highly conserved m^{6}A site (“GGACA”) near the translation initiation region of circ-YAP. Mutation of this single site nearly abolished YAP-220aa production, confirming that one m^{6}A modification is sufficient to enable circRNA translation, consistent with prior reports [22]. Functional assays further showed that only wild-type circ-YAP, and not the m^{6}A -mutant version, enhanced CRC liver metastasis, underscoring the importance of its translational capacity. The modest discordance in expression between circ-YAP and YAP-220aa observed in 7.5% of CRC cases may arise from alterations in m^{6}A regulatory enzymes or components of the translation machinery. Although cytoplasmic localization is generally required for translation, approximately 20% of circ-YAP was detected in the nucleus, implying additional non-coding functions that warrant further exploration.

The Hippo-YAP signaling pathway was originally recognized as an evolutionarily conserved regulator of

organ size control, playing pivotal roles in cell proliferation and differentiation [23]. Accumulating studies have since established that YAP plays critical roles at multiple stages of tumor metastasis. By interacting with TEAD transcription factors, YAP promotes the development of invasive structures, extracellular matrix remodeling, epithelial-mesenchymal transition, and colonization of distant metastatic sites through transcriptional activation of metastasis-related genes [34, 35]. The core Hippo kinase complex suppresses YAP activity by preventing its nuclear entry, primarily through LATS1-dependent phosphorylation at serine 127 and subsequent sequestration in the cytoplasm by 14-3-3 proteins [36]. Although aberrant YAP activation is frequently documented in metastatic cancers [37, 38], the precise molecular mechanisms remain incompletely understood.

In this study, we discovered a novel YAP activator, YAP-220aa, a distinct protein isoform generated by translation of circ-YAP. Despite containing a unique peptide sequence at the circ-YAP junction site ("RPVLMQALQEP"), YAP-220aa retains the complete WW1/2 domain of YAP. This domain is essential for LATS1 binding; therefore, we proposed that YAP-220aa enhances YAP activity by competitively interacting with LATS1. Experimental results confirmed endogenous association between YAP-220aa and LATS1 in CRC cells, leading to decreased YAP phosphorylation and increased nuclear translocation of YAP. Furthermore, genetic silencing of YAP or pharmacological inhibition with verteporfin effectively abolished the pro-metastatic effects of YAP-220aa on CRC liver metastasis, underscoring the dependence of YAP-220aa function on intact YAP signaling. The potential roles of YAP-220aa in other pathological conditions merit additional investigation, and structural studies will be necessary to determine whether its unique junction sequence confers novel functional domains.

Notably, two TEAD-binding motifs were identified in intron 1 of the YAP pre-mRNA upstream of the circ-YAP region. Mutation of these sites eliminated the transcriptional induction of circ-YAP by the YAP/TEAD complex. These observations establish circ-YAP as a direct transcriptional target of YAP, revealing a previously unrecognized positive feedback loop that amplifies the pro-metastatic activity of circ-YAP in CRC and contributes to sustained YAP activation. Given that YAP has historically been regarded as an "undruggable" transcriptional co-activator [39], factors that post-translationally modulate YAP activity may represent its key vulnerability. Our findings describe an endogenous truncated YAP isoform that fine-tunes Hippo-YAP signaling, thereby offering potential new avenues for therapeutic intervention in YAP-driven cancers.

Several limitations should be acknowledged in the current study. The primary constraint is that the in vitro and in vivo experiments relied on conventional two-dimensional human cell lines, which do not fully recapitulate the heterogeneity, clonal evolution, and microenvironmental interactions of clinical tumors. Future work employing advanced three-dimensional organoid models would be valuable. Additionally, the clinical samples and associated data were collected retrospectively, which may introduce biases related to heterogeneous treatment regimens.

Conclusion

In summary, this study reveals a previously unrecognized interplay between a circRNA-encoded protein and the Hippo/YAP signaling pathway, providing new insights and potential therapeutic strategies for the management of CRC liver metastasis.

Acknowledgments: None

Conflict of Interest: None

Financial Support: None

Ethics Statement: None

References

1. Sung H, Ferlay J, Siegel RL, Laversanne M, Soerjomataram I, Jemal A, et al. Global Cancer Statistics 2020: GLOBOCAN estimates of incidence and mortality worldwide for 36 cancers in 185 countries. CA Cancer J Clin. 2021;71(3):209-49.
2. Osei-Bordom DC, Kamarajah S, Christou N. Colorectal cancer, liver metastases and biotherapies. Biomedicines. 2021;9(9):1185.
3. Tsilimigras DI, Brodt P, Clavien PA, Muschel RJ, D'Angelica MI, Endo I, et al. Liver metastases. Nat Rev Dis Primers. 2021;7(1):27.
4. Patop IL, Wust S, Kadener S. Past, present, and future of circRNAs. EMBO J. 2019;38(16):e100836.
5. Kristensen LS, Andersen MS, Stagsted L, Ebbesen KK, Hansen TB, Kjems J. The biogenesis, biology

and characterization of circular RNAs. Nat Rev Genet. 2019;20(11):675-91.
6. Chen X, Zhou M, Yant L, Huang C. Circular RNA in disease: basic properties and biomedical relevance. Wiley Interdiscip Rev RNA. 2022;13(4):e1723.
7. Lei M, Zheng G, Ning Q, Zheng J, Dong D. Translation and functional roles of circular RNAs in human cancer. Mol Cancer. 2020;19(1):30.
8. Kristensen LS, Jakobsen T, Hager H, Kjems J. The emerging roles of circRNAs in cancer and oncology. Nat Rev Clin Oncol. 2022;19(3):188-206.
9. Liu CX, Chen LL. Circular RNAs: characterization, cellular roles, and applications. Cell. 2022;185(12):2016-34.
10. Memczak S, Jens M, Elefsinioti A, Torti F, Krueger J, Rybak A, et al. Circular RNAs are a large class of animal RNAs with regulatory potency. Nature. 2013;495(7441):333-8.
11. Hansen TB, Jensen TI, Clausen BH, Bramsen JB, Finsen B, Damgaard CK, et al. Natural RNA circles function as efficient microRNA sponges. Nature. 2013;495(7441):384-8.
12. Huang A, Zheng H, Wu Z, Chen M, Huang Y. Circular RNA-protein interactions: functions, mechanisms, and identification. Theranostics. 2020;10(8):3503-17.
13. Wang Y, Wu C, Du Y, Li Z, Li M, Hou P, et al. Expanding uncapped translation and emerging function of circular RNA in carcinomas and noncarcinomas. Mol Cancer. 2022;21(1):13.
14. He L, Man C, Xiang S, Yao L, Wang X, Fan Y. Circular RNAs' cap-independent translation protein and its roles in carcinomas. Mol Cancer. 2021;20(1):119.
15. Du WW, Xu J, Yang W, Li X, Li F, Khorshidi A, et al. A neuroligin isoform translated by circNlgn contributes to cardiac remodeling. Circ Res. 2021;129(5):568-82.
16. Gao X, Xia X, Li F, Zhang M, Zhou H, Wu X, et al. Circular RNA-encoded oncogenic E-cadherin variant promotes glioblastoma tumorigenicity through activation of EGFR-STAT3 signalling. Nat Cell Biol. 2021;23(3):278-91.
17. Li Y, Chen B, Zhao J, Li Q, Chen S, Guo T, et al. HNRNPL circularizes ARHGAP35 to produce an oncogenic protein. Adv Sci (Weinh). 2021;8(19):2001701.
18. Wen SY, Qadir J, Yang BB. Circular RNA translation: novel protein isoforms and clinical significance. Trends Mol Med. 2022;28(5):405-20.
19. Jiang X, Liu B, Nie Z, Duan L, Xiong Q, Jin Z, et al. The role of m6A modification in the biological functions and diseases. Signal Transduct Target Ther. 2021;6(1):74.
20. Zeng K, Chen X, Hu X, Liu X, Xu T, Sun H, et al. LACTB, a novel epigenetic silenced tumor suppressor, inhibits colorectal cancer progression by attenuating MDM2-mediated p53 ubiquitination and degradation. Oncogene. 2018;37(41):5534-51.
21. Li S, Li X, Xue W, Zhang L, Yang LZ, Cao SM, et al. Screening for functional circular RNAs using the CRISPR-Cas13 system. Nat Methods. 2021;18(1):51-9.
22. Yang Y, Fan X, Mao M, Song X, Wu P, Zhang Y, et al. Extensive translation of circular RNAs driven by N(6)-methyladenosine. Cell Res. 2017;27(5):626-41.
23. Moya IM, Halder G. Hippo-YAP/TAZ signalling in organ regeneration and regenerative medicine. Nat Rev Mol Cell Biol. 2019;20(4):211-26.
24. Ibar C, Irvine KD. Integration of Hippo-YAP signaling with metabolism. Dev Cell. 2020;54(2):256-67.
25. Kong S, Tao M, Shen X, Ju S. Translatable circRNAs and lncRNAs: driving mechanisms and functions of their translation products. Cancer Lett. 2020;483:59-65.
26. Plawgo K, Raczynska KD. Context-dependent regulation of gene expression by non-canonical small RNAs. Noncoding RNA. 2022;8(4):55.
27. Misir S, Wu N, Yang BB. Specific expression and functions of circular RNAs. Cell Death Differ. 2022;29(3):481-91.
28. Yang Q, Li F, He AT, Yang BB. Circular RNAs: expression, localization, and therapeutic potentials. Mol Ther. 2021;29(5):1683-702.
29. Wang S, Latallo MJ, Zhang Z, Huang B, Bobkov DG, Tigano M, et al. Nuclear export and translation of circular repeat-containing intronic RNA in C9ORF72-ALS/FTD. Nat Commun. 2021;12(1):4908.
30. Deng LJ, Deng WQ, Fan SR, Chen MF, Qi M, Lyu WY, et al. m6A modification: recent advances, anticancer targeted drug discovery and beyond. Mol Cancer. 2022;21(1):52.

31. Zhang F, Liu H, Duan M, Wang G, Zhang Z, Wang Y, et al. Crosstalk among m(6)A RNA methylation, hypoxia and metabolic reprogramming in TME: from immunosuppressive microenvironment to clinical application. J Hematol Oncol. 2022;15(1):84.
32. Frye M, Harada BT, Behm M, He C. RNA modifications modulate gene expression during development. Science. 2018;361(6409):1346-9.
33. Niu X, Yang Y, Ren Y, Zhou S, Mao Q, Wang Y. Crosstalk between m(6)A regulators and mRNA during cancer progression. Oncogene. 2022;41(39):4407-19.
34. Li HL, Li QY, Jin MJ, Sun YC, Zhao Y, Wang X, et al. A review: hippo signaling pathway promotes tumor invasion and metastasis by regulating target gene expression. J Cancer Res Clin Oncol. 2021;147(6):1569-85.
35. Zanconato F, Cordenonsi M, Piccolo S. YAP and TAZ: a signalling hub of the tumour microenvironment. Nat Rev Cancer. 2019;19(8):454-64.
36. Zhao B, Li L, Tumaneng K, Wang CY, Guan KL. A coordinated phosphorylation by Lats and CK1 regulates YAP stability through SCF(β-TRCP). Genes Dev. 2010;24(1):72-85.
37. Warren J, Xiao Y, Lamar JM. YAP/TAZ activation as a target for treating metastatic cancer. Cancers (Basel). 2018;10(4):115.
38. Tocci P, Blandino G, Bagnato A. YAP and endothelin-1 signaling: an emerging alliance in cancer. J Exp Clin Cancer Res. 2021;40(1):27.
39. Yan F, Qian M, He Q, Zhu H, Yang B. The posttranslational modifications of Hippo-YAP pathway in cancer. Biochim Biophys Acta Gen Subj. 2020;1864(2):129397.